Journal of
Mechanical
Science and
Technology

Journal of Mechanical Science and Technology 21 (2007) 1408~1414

Vortex-induced Vibration Control by Micro Actuator

Bao-Qing Li[a, b], Yang Liu[b,*], Jia-Ru Chu[a]

[a]*Department of Precision Machinery and Precision Instrumentation*
University of Science and Technology of China Hefei, Anhui, China
[b]*Department of Mechanical Engineering, The Hong Kong Polytechnic University,*
Hung Hom, Kowloon, Hong Kong

(Manuscript Received October 20, 2006; Revised March 30, 2007; Accepted May 2, 2007)

Abstract

The control of vortex-induced vibration of two side-by-side circular cylinders in a cross flow is carried out experimentally. One cylinder is elastically supported and the other is fix-supported at both ends. The two cylinders vibrate under the action of the unsteady flow-induced forces. A micro actuator is embedded on the surface of each cylinder to perturb the boundary layer. The spacing ratio is set at 1.2. The measurement shows that the structural vibration can be suppressed significantly when the reduced excitation frequency is around 2.655.

Keywords: Control; Vortex-induced vibration; PZT actuator

1. Introduction

For the structure in a cross flow, the shed vortices would generate oscillating forces, which in turn cause the structures to vibrate. The resultant vibration can influence the flow field and vortex shedding, especially when the structural natural frequency is at or near the vortex shedding frequency. The vortex-induced vibration (VIV) is of practical importance because of its potentially destructive effect to structures, such as bridges, stacks, towers, offshore pipelines, and heat exchangers. The practical significance of VIV has led to a large number of fundamental studies, many of which were discussed in comprehensive reviews or books (Bearman, 1984; Blevins, 1990; Sumer and Fredsoe, 1997; Jauvtis and Williamson, 2004).

To reduce or eliminate the potential disaster by VIV, many methods have been proposed to reduce the vortex-induced vibration. They can be categorized into passive control and active control. The passive methods such as using the axial slats and the splitter plate to change the structure's formation (Zdravkovich, 1981; Wong and Kokkalis, 1982; Wilson and Tinsley, 1989), can effectively suppress the vortex-induced vibration, which have been successfully applied in wind and marine engineering. On the other hand, active control methods influence the fluid-structures by using actuators driven by external energies (Baz and Ro, 1991; Cheng and Zhou, 2003). For existing VIV control strategies, they can be categorized into structural vibration control and flow control which tends to modulate vortex shedding and subsequently suppresses vortex-induced vibration.

The earliest and most lasting actuator may be acoustic actuator due to its convenient advantage which has been used since 1960s. Both external and internal acoustic excitations were used for flow control (Bloors, 1964; Ahuja et al., 1983; Fujisawa and Takeda, 2003). It was found that when the excitation's frequency, position and amplitude were optimized, drag could be reduced and the vortex shedding could be weakened significantly. Some of

*Corresponding author. Tel.: +852 2766 7814, Fax.: +852 2365 4703
E-mail address: mmyliu@polyu.edu.hk

the researchers consider the exciting frequency is most effective at instability frequency existed in shear layer. Baz and Ro (1991) used an electromagnetic actuator, placed at critical location inside the cylinder to resist the flow-induced vibration. The actuator was powered by a feedback signal proportional and opposite to the velocity of the cylinder, and could effectively reduce vibration of 80%. For most of the active control techniques, either the power of the excitation source is quite high or the area of the excitation is quite wide compared to the whole structure, which limit their practical applications.

MEMS actuators have recently made their way to the forefront of flow control research. Flow control is most effective when applied near the transition or separation points, *i.e.*, near the critical flow regimes where flow instabilities amplify quickly. This is especially important for micro actuators because these actuators cannot deliver large forces or high power. The matching in length scale between the micro transducers and the structures makes the manipulation of these structures possible (Ho and Tai, 1998; Lofdahl and Gad-el-Hak, 1999). Therefore, MEMS-based transducers can be applied in flow-induced vibration problems to help find a way to achieve a more efficient way to control vibration and thus prevents the possible occurrence of disasters in many engineering systems.

In this study, a type of micro actuator is used to control the flow-induced vibration of two side-by-side cylinders with spacing ratio of $T/d = 1.2$ (T is the center-to-center distance between the cylinders and d is the diameter of the cylinder). The objective is to use small device (both in size and power) to control vortex shedding then control vibration of larger structures.

2. Experimental details

2.1 Experimental setup

The experiments were performed in a closed-circuit wind tunnel in which the test section measures *0.6 m* by *0.6 m*. The flow velocity ranges from *2* to *50 m/s*, the streamwise mean velocity uniformity is *0.1%*, and the turbulence intensity is no more than *0.4%*.

Two acrylic tubes each with an embedded actuator were placed side-by-side in a cross flow Fig. 1(a). The outer diameter is $d = 25$ *mm* and the thickness of the tube is *3 mm*. Length of the cylinder is $L = 700$ *mm*. One of the cylinders is rigidly mounted on the walls of the wind tunnel, and the other is spring-supported via a block on each end. The transverse center-to-center spacing ratio is set as $T/d = 1.2$. As shown in Fig. 1(b), the block mated with cylinder is supported by three compression springs. The mid-spring with spring constant $K_1 = 1500$ *N/m* is mounted at both ends and then it is fixed. The other two springs with spring constant $K_2 = K_3 = 100$ *N/m* are removable in the gap in order to balance the influence of the drag force and the induced oscillation in the streamwise direction. The definition of coordinate system (x, y, z) and azimuth angle (θ) are shown in Figs. 1(a) and 1(c), and the angle describes the location of the actuators.

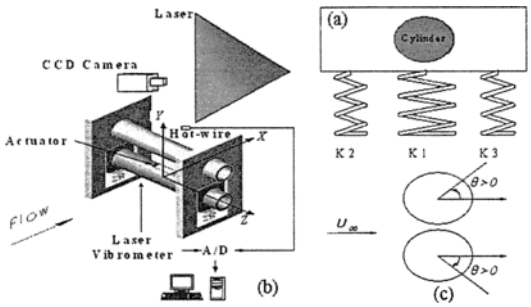

Fig. 1. (a) Schematic view of experimental setup, (b) enlarged view of elastic support, (c) definition of angle.

2.2 The micro actuator and its installation

The in-house made piezoelectric ceramic actuator was installed in a cavity which is inscribed by laser on cylinder surface. As shown in Fig. 1(a), the actuator is located in the middle of the cylinder. The length of the actuator is *20 mm*, and the area of the cross section is *1 mm* × *0.5 mm*. The cavity's size is *20.5mm* × *1.5mm* × *1mm*, in which the actuator is stuck on a 2 mm-length step and vibrates freely as a cantilever beam. Therefore, the ratio of the working length between actuator and cylinder is $18/600 \approx 3\%$.

The actuator is composed of five layers, i.e., upper electrode, PZT, middle electrode, PZT and lower electrode, as shown in Fig. 2. The outer electrode is a thin layer of metal powder which is coated on the PZT layer that has a combined thickness of *0.2 mm*. And the middle electrode is a *0.1 mm*-thickness copper sheet. The upper and lower electrodes are in short circuit, and the two PZT layers are polarized in the same direction. This can ensure that, when a voltage is applied between the middle and the upper electrodes, the two electric fields in PZT layers are

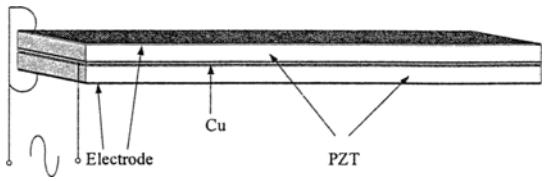

Fig. 2. Schematic view of the actuator's structures.

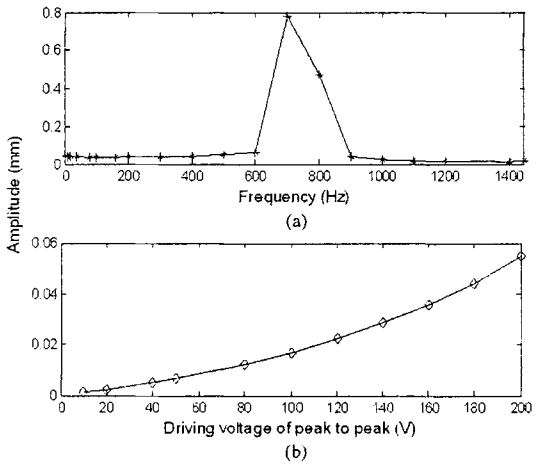

Fig. 3. Vibration amplitude of actuator under different conditions. (a) At different driving frequencies, and (b) at different driving voltages.

opposite. Owning to the characteristics of PZT material, one layer would extend its length, while the other layer would contract lengthwise. That makes the cantilever beam bend toward one side. Changing the direction of the applied voltage would induce the beam to bend toward the other side. If an alternating voltage is applied, the cantilever beam could vibrate continuously.

Figure 3 shows the performance of actuator driven by sinusoidal signals. The signal is generated from a signal generator, and then amplified by a PZT amplifier (TRE-603). There is a resonance region around *700 Hz*, below this resonance region, the vibrating amplitude of cantilever end is about *40 μm* at driving voltage of *200 V*. A wide range of frequencies were tested and it is found the most effective driving frequency was f = *595 Hz*. Figure 3(b) shows that the vibration amplitude is monotonically increased with increasing driving voltages at *595 Hz*. In this study, the driving voltage was set at 200 *V*.

2.3 Measurement facility

Unsteady flow measurements are obtained with a hot-wire anemometer which is located at x/d = *4*, y/d = *-0.5*, z/L = *0*. Transverse cylinder vibration is measured by the Polytec Series 3000 Dual Beam Laser Vibrometer that is focused on the spring-supported cylinder. A 12-bit A/D board simultaneously sampled the vibration and flow velocity signals.

The velocity field is measured using a Dantec standard PIV2100 system with a Dantec FlowMap Processor. The smoke with a particle size around 1 *μm* is seeded into the flow, which is generated from paraffin oil. The flow is illuminated by two New Wave standard pulsed laser sources with wavelength of *532 nm*, each having a maximum energy output of *120 mJ*. A wide-angle lens is used so that each image coveres an area over *160 mm* × *120 mm* of the flow field. The images are taken by the CCD camera (HiSense type 13, *1280 pixels* × *1024 pixels*). The cross-correlation between two consecutive images is calculated with the interrogation area of *64 pixels* × *64 pixels* and a 50% overlap, which is used to minimize the occurrence of erroneous vectors.

3. Results and discussion

The most effective vibration control is to suppress the oscillation at cylinder resonance. In this paper, the reduced frequency f^*, reduced exciting frequency f_e^*, reduced natural frequency f_n^* and reduced shedding frequency f_s^* are defined as

$$f^* = \frac{f\,d}{U_\infty} \tag{1}$$

$$f_e^* = \frac{f_e d}{U_\infty}, \tag{2}$$

$$f_n^* = \frac{f_n d}{U_\infty}, \tag{3}$$

$$f_s^* = \frac{f_s d}{U_\infty}, \tag{4}$$

respectively. Where f_e, f_n and f_s are the excitation frequency, natural frequency and shedding frequency, respectively. The reduced structural natural frequency f_n^* = *0.092*, therefore the flow parameters are chosen as $f_s^* = f_n^*$ = *0.092*, where *Re* = *9272* and U_∞ = *5.6 m/s*.

It has been well-know that flow control is most effective when applied near the transition or

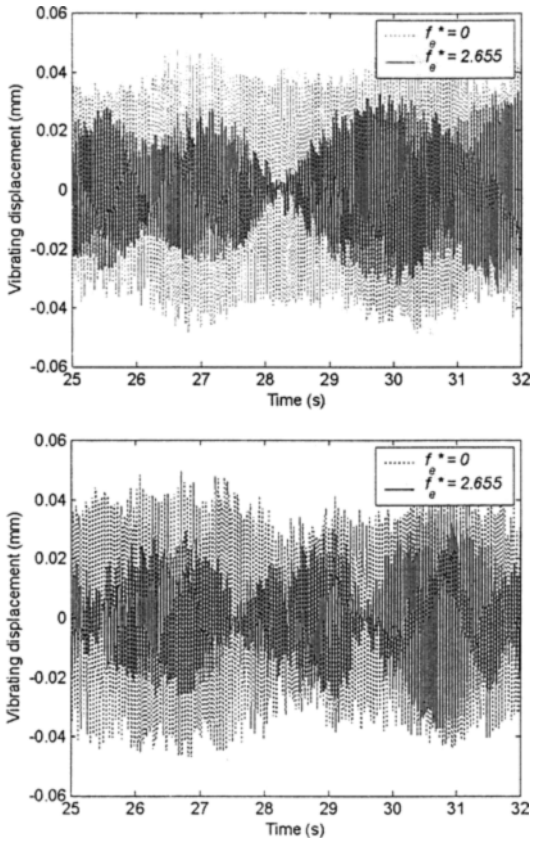

Fig. 4. Comparison of vibration time histories of cylinders between without and with excitation at $\theta=95^o$ (up) and $\theta=100^o$ (down).

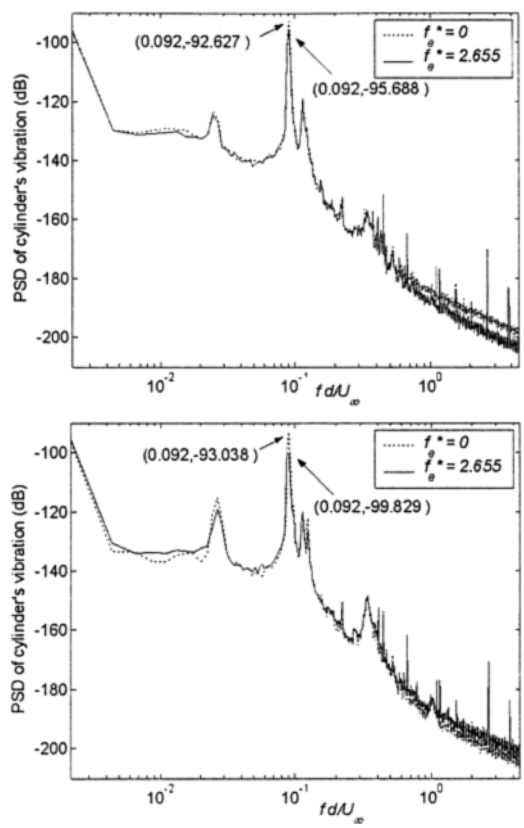

Fig. 5. Comparison of PSD analyses of vibration between without and with excitation at $\theta = 95^o$ (up) and $\theta = 100^o$ (down).

separation points Ahuja et al. (1983), Hsiao and Shyu (1991). The flow instabilities can be amplified quickly near these critical regions. In this study, the actuators' locations are adjusted between $\theta = 95^o$ and 100^o which is within the separation region. Figure 4 presents the comparison of cylinder vibration time series with and without actuator excitations. Without excitation, i.e., $f_e^* = 0.0$, the amplitude is stable at about $40\ \mu m$; when actuators work, i.e., $f_e^* = 2.655$, the amplitude decreases at least $10\ \mu m$ for both $\theta = 95^o$ and 100^o, and there exist a strong beating phenomenon with actuator excitations. Comparison of power spectral density (PSD) of vibration amplitude provides more insight into the phenomenon. Figure 5 shows that there exist three dominant peaks in the PSD plot, i.e., $f^* = 0.025,\ 0.092$ and 0.116. The first peak is induced by streamwise oscillation of the circular cylinder, and the rest two peaks are the natural frequencies of the elastic supports at both ends. For $\theta = 95^o$, the PSD at $f_n^* = 0.092$ reduces $3\ dB$ with actuator excitation, equivalent to 50% reduction of energy; for $\theta = 100^o$, the reduction is $6.8\ dB$ at $f_n^* = 0.092$, which is equivalent to 80% energy reduction compare to the case of without excitation.

The PIV visualization in the cylinder wake provides additional information on the wake control by the MEMS actuators. Figure 6 shows the comparison of vorticity distribution at $\theta = 95^o$. Without excitation, i.e., $f_e^* = 0.0$, the two cylinders behave like a single bluff body, the vorticity is quite strong and the vortexes shed from the outer sides of the two cylinders; with excitation, the wake length becomes longer and the vorticity becomes weak. This indicates that the excitation of MEMS actuator has changed the wake characteristics.

We performed additional vibrometer and hot-wire measurements to investigate the instantaneous effect of the PZT actuators. This is shown in Figure 7 where the excitation frequency is $f_e^* = 2.655$ at $6\ s < t < 38\ s$ and there is no excitation beyond this time span. It

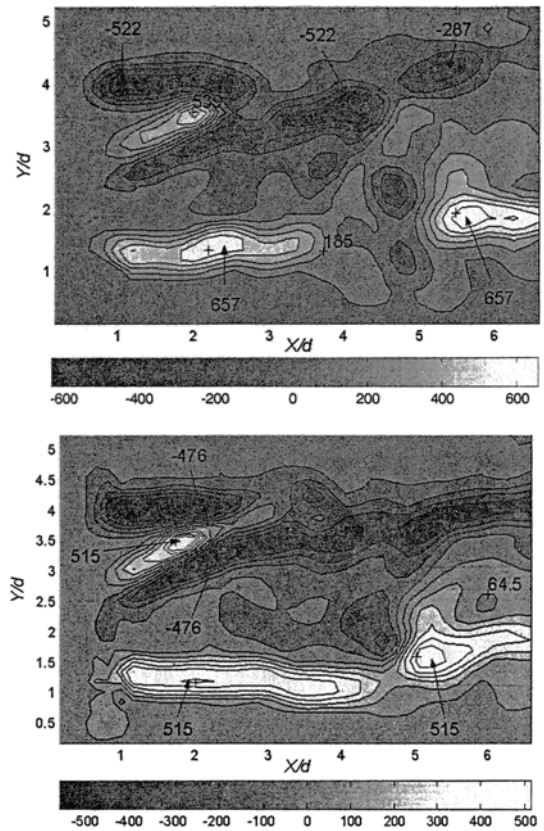

Fig. 6. Vorticity distribution by PIV measurement at $f_e^* = 0.0$ (up) and $f_e^* = 2.655$ (down), where cylinders are at the left side ($\theta = 95°$).

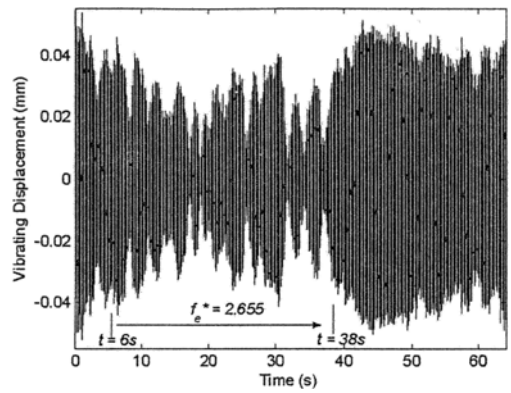

Fig. 7. Instantaneous effect of excitation on time history of vibration (θ=95°).

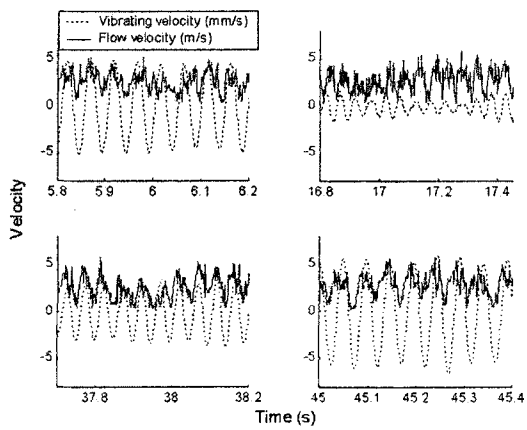

Fig. 8. Comparison of velocity oscillations between vibrating velocity of cylinder and flow velocity.

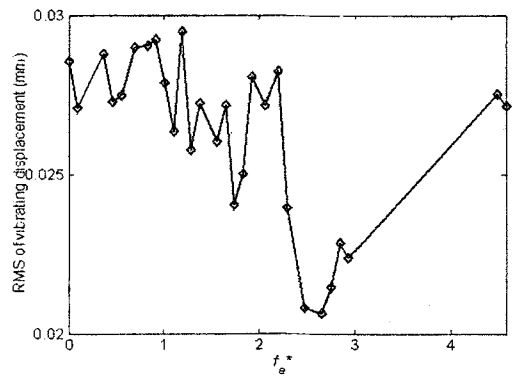

Fig. 9. RMS amplitude of vibration at different exciting frequencies (θ=95°).

can be seen that as soon as the excitation works, the time series immediately becomes beating and the amplitude reduces apparently. Figure 8 shows the comparison of cylinder vibrating velocity and near-wake flow velocity within the same period of time as in Fig. 7. At $t < 6$ s, when there is no excitation, the two time series are almost in-phase. Within the excitation period, as shown during $16.8\ s < t < 17.4\ s$ in Fig. 8, the two signals intermit between in-phase and out-of-phase, and the vibrating amplitude is suppressed significantly. When the excitation stops, i.e., when $t > 38$ s, the two signals change back to in-phase again, and the vibrating amplitude increases back.

Figure 9 shows the root mean square (RMS) of vibration amplitude with different excitation frequencies at $\theta = 95°$. There exists a minimum at around $f_e^* = 2.655$ and it is also true for other excitation angles, therefore, the optimum excitation frequency was set at $f_e^* = 2.655$ during experiments.

Flow control is most effective when the excitation is applied near the separation points. Since the boundary separation is an unsteady process, and the point is varying within a range, it is difficult to catch

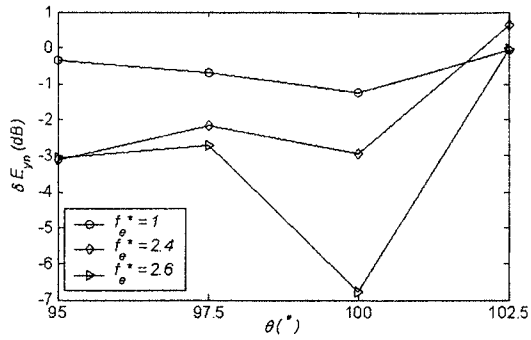

Fig. 10. The reduction of E_{yn} at different exciting locations (E_{yn} is the PSD of vibration at the natural frequency. δE_{yn} is defined as the difference of E_{yn} between with and without exciting).

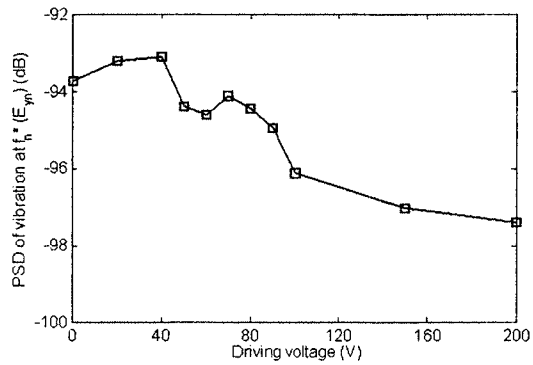

Fig. 11. PSD of vibration (E_{yn}) at different driving voltage (θ=95°).

the exact separation point during experiment. Figure 10 shows the control effects at different locations near separation region. The results indicate that the effective control region is around $95° \leq \theta \leq 100°$ and the most effective location is at $\theta = 100°$.

From above discussion, it has been known that the excitation location and frequency are crucial for effective flow control, but the excitation amplitude is also a very important parameter in flow control. Figure 11 shows the variation of PSD of vibrating amplitude at reduced natural frequency f_n^* with different driving voltage. The vibration energy begins to decrease at driving voltage of *50V*; with increasing the driving voltage to *100V*, the vibration energy decreases *50%*. Further increasing driving voltage, the vibration energy does not reduce significantly, indicating the critical driving voltage is about 100V which is equivalent to the actuator excitation amplitude of *16.6 μm*. Generally speaking, the higher excitation amplitude is, the better control effect is.

4. Conclusions

A micro actuator made of PZT material is used to control the vortex-induced vibration of two side-by-side cylinders. The embedded actuator works as a cantilever beam, perturbs the boundary layer periodically when driven by a sinusoidal signal. Results indicate that vibration of cylinder could be suppressed by micro-excitation of PZT actuators, and the reduction is rather sensitive to the actuators' exciting frequency, location and amplitude. The analyses of the measurements lead to the following conclusion:

(1) The excitation frequency has significant influence on the fluid-structure control, and there exists an optimum excitation frequency. The most effective reduced excitation frequency is $f_e^* = 2.655$ for current experimental setup, and the vibration energy can be decreased *80%*.

(2) The most effective location of the excitation should be near the boundary separation point, for the two side-by-side cylinders at spacing ratio of 1.2, the optimum location is at $\theta = 100°$.

(3) The excitation amplitude is also crucial for the wake control. There is a critical actuator excitation amplitude, below this amplitude, the cylinder vibration can not be suppressed greatly; and above this amplitude, the cylinder vibration decreases slowly.

Acknowledgements

Support given by the Research Grants Council of the Government of the HKSAR under Grant No. PolyU 5305/03E, and by The Hong Kong Polytechnic University under Central Research Grant No. A-PE53 and G-U076 is gratefully acknowledged.

References

Ahuja, K. K., Whipkey, R. R. and Jones G. S., 1983, "Control of Turbulent Boundary Layer Flows by Sound," *AIAA Paper*, pp. 83-0726.

Baz, A. and Ro, J., 1991, "Active Control of Flow-induced Vibrations of a Flexible Cylinder using Direct Velocity Feedback," *Journal of Sound and Vibration*, Vol. 146, pp. 33-45.

Bearman, P. W., 1984, "Vortex Shedding from Oscillating Bluff Bodies," *Annual Review of Fluid Mechanics*, Vol. 16, pp. 195-222.

Blevins, R. D., 1990, "Flow-induced Vibration," 2nd edition, New York.

Bloors, M. S., 1964, "The Transition on Turbulence

in the wake of a Circular Cylinder," *Journal of Fluid Mechanics,* Vol. 19, pp. 290-303.

Cheng, L., Zhou, Y., Zhang M. M., 2003, "Perturbed Interaction between Vortex Shedding and Induced Vibration," *Journal of Fluids and Structures*, Vol. 17, pp. 887-901.

Fujisawa, N. and Takeda, G., 2003, "Flow Control Around a Circular Cylinder by Internal Acoustic excitation," *Journal of Fluids and Structures,* Vol. 17, pp. 903-913.

Ho, C. M. and Tai, Y. C., 1998, "Micro-Electro-Mechanical-Systems (MEMS) and Fluid Flows," *Annual Review of Fluid Mechanics*, Vol. 30, pp. 579-612.

Hsiao, F. B. and Shyu, J. Y., 1991, "Influence of Internal Acoustic Excitation upon flow Passing a Circular cylinder," *Journal of Fluids and Structures,* Vol. 5, pp. 427-442.

Jauvtis, N. and Williamson, C. H. K., 2004, "The Effect of Two Degrees of Freedom on Vortex-induced Vibration at Low Mass and Damping," *Journal of Fluid and Mechanics*, Vol. 509, pp. 23-62.

Lofdahl, L. and Gad-el-Hak, M., 1999, "MEMS Applications in Turbulence and Flow Control." *Progress in Areospace Science*, Vol. 35, pp. 101-203.

Sumer, B. M. and Fredsoe, J., 1997, "Hydrodynamics around Cylindrical Structures. "Singapore: *World Scientific*.

Wong, H. Y., Kokkalis A., 1982, "A Comparative study of three Aerodynamic Devices for Suppressing Vortex-induced Oscillation," *Journal of Wind Engineering and Industrial Aerodynamics*, Vol. 10, pp. 21-29, 1982.

Wilson, J. E. and Tinsley J. C., 1989, "Vortex load Reduction; Experiments in Optimal Helical Strake Geometry for Rigid Cylinders," *Journal of Energy Resources Technology*, Vol. 3, pp. 71-76.

Zdravkovich, M. M., 1981, "Review and Classification of Various Aerodynamic and Hydrodynamic means for Suppressing Vortex Shedding Vortex Shedding," *Journal of Wind Engineering and Industrial Aerodynamics*, Vol. 7, pp. 145-189.